THE JOURNAL OF PHYSICAL CHEMISTRY C

Article

Cite This: J. Phys. Chem. C 2019, 123, 15738−15743

pubs.acs.org/JPCC

Probing the Effect of Chemical Dopant Phase on Photoluminescence of Monolayer MoS_2 Using in Situ Raman Microspectroscopy

Blake Birmingham,[†,‡] Jiangtan Yuan,[§] Matthias Filez,[∥] Donglong Fu,[∥] Jonathan Hu,[⊥] Jun Lou,[§] Marlan O. Scully,[‡] Bert M. Weckhuysen,[∥] and Zhenrong Zhang*[,†]

[†]Department of Physics and [⊥]Department of Electrical and Computer Engineering, Baylor University, Waco, Texas 76706, United States

[‡]Institute for Quantum Science and Engineering, Texas A&M University, College Station, Texas 77843, United States

[§]Department of Materials Science and NanoEngineering, Rice University, Houston, Texas 77005, United States

[∥]Inorganic Chemistry and Catalysis group, Utrecht University, Universiteitsweg 99, 3584 CG Utrecht, The Netherlands

Supporting Information

ABSTRACT: Understanding the role of chemical dopants is crucial to modulating the optoelectronic properties of monolayer (ML) MoS_2 and realizing its optoelectronic applications such as photodetectors, switching devices, and ultrathin transistors. Here, the effect of the dopant phase of the same dopants—liquid and gaseous—on the optical properties of ML MoS_2 has been investigated using in situ Raman microspectroscopy with an environment-controlled reaction cell. The results show that the gaseous n-type dopant, that is, pyridine, completely quenched the PL intensity of ML MoS_2, while liquid pyridine preserved 50% of the original PL intensity attributed to its less effective charge transfer to MoS_2 than the gaseous counterpart. Photoemission of the quenched MoS_2 could not be recovered with mild annealing in nitrogen and only partially recovered upon long-term exposure to air. The results show that the dopant phase strongly impacts the PL properties of ML MoS_2.

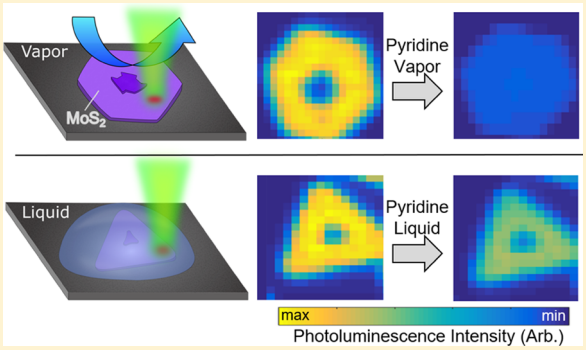

INTRODUCTION

Chemical doping has been proven crucial for engineering the optoelectronic properties of monolayer (ML) MoS_2 for applications such as ultrathin MoS_2 transistors, photodetectors, and switching devices.[1−7] Recently, single-layer-based MoS_2 field-effect transistors have benefited from an increased carrier concentration modulated by adsorbate and impurity engineering.[8,9] MoS_2 has also been proven to be a potential candidate in the step toward a hydrogen-based economy by improving both photovoltaic energy generation and hydrogen-evolution-based energy storage systems due to the monolayer's direct band gap and visible light absorption properties.[10,11] Both gas- and solution-based doping methods have been developed to modify the photoluminescence (PL) intensity of ML MoS_2.[2−7,12−15] However, the impact of the phase (liquid vs gaseous) of the chemicals in chemical doping has not been addressed.

Chemical vapor doping has been utilized for effective sensing of an electron-donor analyte[13] and for the modulation of PL through charge carrier doping.[12] In chemical vapor sensing, the chemical vapor affects both PL and conductivity. Indeed, recently, it has been shown that strong electron-donor chemical vapor analytes can induce a semiconductor−metal 2H−1T phase transition, similar to the chemical exfoliation of transition-metal dichalcogenides, which leads to the formation of a metallic 1T phase.[16−19] The 1T phase has been proven to have superior catalytic efficiency for hydrogen evolution reactions over the 2H semiconductor phase in part due to increased conductivity.[20,21]

Besides gas-phase doping, solution-based chemical doping is also known as an effective but convenient method to modify the carrier density of ML materials.[2−7,14,15] Mouri et al. demonstrated the tunable PL properties of ML MoS_2 via different types of dopants using a solution-based chemical doping technique.[13] Adsorption of p-type dopants drastically enhanced the PL intensity of ML MoS_2. This intensity enhancement was explained by the switching of the dominant PL process from the recombination of negative trions to the recombination of neutral excitons through extraction of the unintentionally high doped electrons. On the other hand, adsorption of n-type dopants could reduce the PL intensity, which was attributed to the suppression of neutral exciton PL through injection of excess electrons.[7,13] These experiments

Received: April 9, 2019
Revised: June 7, 2019
Published: June 8, 2019

DOI: 10.1021/acs.jpcc.9b03277
J. Phys. Chem. C 2019, 123, 15738−15743

were performed on mechanically exfoliated ML MoS_2 on SiO_2/Si substrates.

While numerous studies investigate variation of the PL properties of MoS_2 MLs by gas-phase or liquid-phase doping separately, a direct comparison of gas- and liquid-phase doping with the same chemical has been rarely reported. Here, we report the effect of the phase of electron-donor chemicals on the chemical doping of MoS_2 by using in situ Raman microspectroscopy equipped with a reaction cell to monitor the optical properties of MoS_2 upon vapor doping, liquid doping, and annealing. We found that the gas-phase n-type dopant, that is, pyridine, completely quenches the PL intensity of ML MoS_2 via charge transfer from pyridine to MoS_2. Interestingly, liquid pyridine is much less effective than gaseous-phase pyridine in quenching the PL intensity of ML MoS_2. The chemical doping is further studied by thiophene, a weaker n-type dopant.

■ EXPERIMENTAL METHODS

Monolayer 2H-MoS_2 flakes were synthesized using the CVD method reported in previous work.[22] Briefly, an alumina boat containing MoO_3 powder as a growth precursor was put in the center of a furnace heating zone. A clean SiO_2/Si substrate was put on top of the boat with the SiO_2 side facing the precursor. Sulfur powder was placed in the upstream zone of the tube furnace. The tube was purged with argon for 15 min, and the growth was maintained at 750 °C for 40 min under the protection of argon. The furnace was then cooled to room temperature naturally.

The CVD-grown MoS_2 samples were exposed to pyridine or thiophene vapor inside an in situ reaction cell (Linkam Scientific THMS600) in which the gas flow rate could be finely controlled. The samples were positioned in the reaction cell on a scanning Raman microscope to in situ monitor the change of the optical spectra. The Raman microscope consisted of a 532 nm laser and a Renishaw inVia Raman spectrometer coupled with a Leica confocal microscope. PL spectra were detected through a 1200 line/mm grating using continuous rotation to acquire spectra in the 500−725 nm range. Raman spectra were acquired with a stationary grating. All presented MoS_2 PL and Raman spectra were acquired with a 20× oil-based objective with a laser spot size near 1.5 μm directed through a quartz view port on the reaction cell. The laser power at the sample was around 40 μW with power density near ∼100 $\mu W/cm^2$ to prevent damage to the flakes caused by local heating.[23] Monolayer flakes were identified using optical contrast in an optical microscope and confirmed using microspot (∼1.5 μm) PL, Raman spectroscopy, and atomic force microscope measurements.[23]

Prior to placing the sample into the cell, the cell was baked overnight in air to eliminate any effect from the chemical residue. The PL map and Raman map were taken in the closed reaction cell in air at room temperature through a quartz window before the chemical doping. To avoid the effect of photoinduced reactions in air on the PL intensity of the flake,[23] only one set of PL map and Raman map were taken on each targeted flake before exposure. Flakes were then exposed to the gaseous chemical dopant (pyridine or thiophene). Exposure was controlled by a saturator flow cell in which nitrogen gas was bubbled through the liquid dopant at a flow rate of 40 mL/min to carry the dopant vapor through the cell. PL maps and Raman maps were acquired on the MoS_2 flakes after the sample in the reaction cell was in dopant vapor for 5 min. After gaseous exposure, samples were heated in situ to 150 °C for 30 min in nitrogen at a flow rate of 40 mL/min. The maps were taken after the samples cooled down to room temperature in nitrogen at a flow rate of 60 mL/min.

For liquid chemical doping, a droplet of pyridine was pipetted onto the flakes, and the pyridine evaporated within 5 min with nearby fume extraction. To keep the pyridine−MoS_2 interaction times similar in the liquid and gas exposure cases, the MoS_2 flakes were exposed to gaseous pyridine for approximately the same amount of time (5 min) as was required for the liquid pyridine to completely evaporate from the sample surface. The PL maps and Raman maps were taken in the prebaked reaction cell before and after liquid pyridine exposure and evaporation at room temperature in air through a quartz window to keep the laser power consistent with gas-phase experiments.

■ RESULTS AND DISCUSSION

The optical image (Figure 1a) shows ML MoS_2 with a bilayer at the center of the flake. Before pyridine exposure, there is a strong PL emission from the pristine ML MoS_2 flake on silica (Figure 1b). The bilayer MoS_2 shows a much lower PL intensity as expected due to the deviation from the direct band gap.[24,25] The PL emission from the interior of the ML flake is mostly uniform and shows a higher intensity than the edge region of the flake. The results are consistent with previously reported PL maps measured on CVD-grown MoS_2 flakes using near-field scanning microscopy.[26]

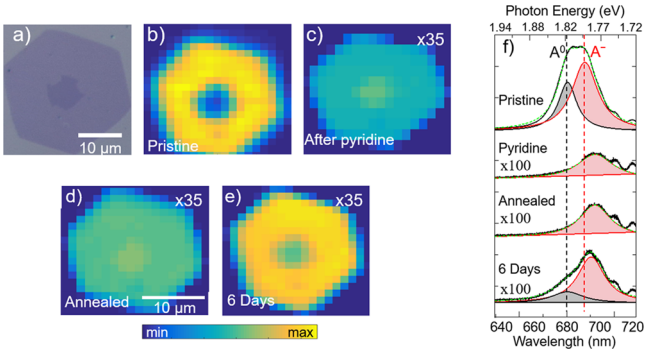

Figure 1. Quenching of monolayer MoS_2 photoluminescence (PL) emission by gaseous pyridine exposure and PL recovery. (a) Optical image of a pristine MoS_2 flake on SiO_2/Si substrate. PL map of the same flake before (b) and after (c) exposure to gaseous pyridine. (d) PL map of the same MoS_2 flake post annealing at 150 °C for 30 min in N_2 and (e) after 6 days in air. The image intensity of panels (c−e) is 35 times the raw intensity to show the contrast. (f) Representative PL spectra of the pristine monolayer MoS_2 flake, pyridine-dosed flake, annealed, and flake exposed to air for 6 days. The dashed green line is the fit of the PL spectra with deconvoluted A^0 and A^- shown as the gray and red infill, respectively.

Upon exposure to gaseous pyridine, the PL of the same MoS_2 flake (Figure 1c) is nearly completely quenched over the entirety of the flake. Exposure resulted in a greater than 99% decrease in the overall PL of the ML. The PL map shows that the PL emission was uniformly quenched across the entire ML flake (Figure 1c). The PL intensity from the bilayer is quenched slightly less than the ML emission with a 95% decrease and is now 10% brighter than the ML PL.

Additional to the decrease in PL intensity upon exposure of gaseous pyridine, the emission bands are quenched differ-

DOI: 10.1021/acs.jpcc.9b03277
J. Phys. Chem. C 2019, 123, 15738−15743

entially. There are two reported PL bands from ML MoS_2, namely, A exciton at 670 nm (~1.85 eV) and B exciton at 615 nm (~2.02 eV).[27] They are associated with direct optical transitions from the lowest conduction bands to the highest spin-split valence bands.[28−30] A exciton spectra can be deconvoluted into two bands, namely, neutral A^0 exciton and negative A^- multiexciton. The A exciton peak is clearly nonsymmetric and shows the existence of multiexcitons before the exposure (Figure 1f). After exposure, there is a complete suppression of the neutral A^0 exciton band and a significant quenching (~99%) of the A^- trion emission from the ML MoS_2. The peak position of the remaining A^- trion emission is redshifted by 8 nm (~0.016 eV) immediately upon exposure. The quenched MoS_2 photoemission is not reversible with mild annealing in nitrogen. After annealing at 150 °C for 30 min, the PL recovered only 1% of its initial intensity uniformly over the ML flake (Figure 1d), and only the trion portion of the emission recovered (Figure 1f).

It has been reported that physisorbed pyridine desorbs in vacuum below room temperature and pyridine does not adsorb on MoS_2 at room temperature either on the basal plane or on the edge sites.[31] We did not detect any pyridine Raman signal on MoS_2 upon gaseous pyridine exposure (Figure 2), though

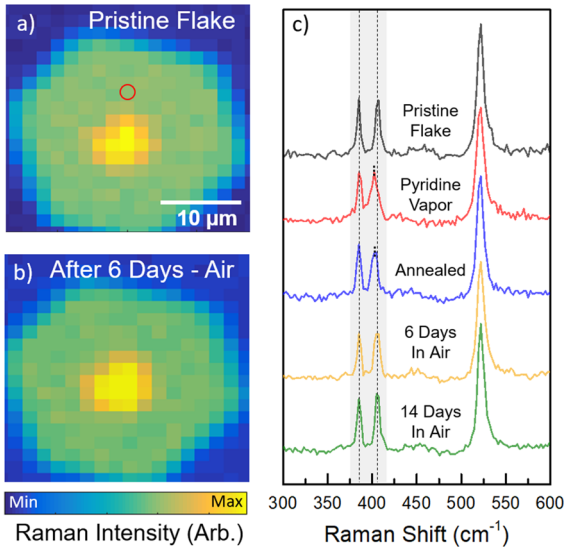

Figure 2. MoS_2 Raman maps and spectra. Raman intensity maps of (a) pristine MoS_2 flake on a SiO_2/Si substrate and (b) the same flake after subsequent exposure to pyridine vapor, annealing, and 6 days of exposure to atmospheric conditions. (c) Typical Raman spectra of monolayer (upper middle portion of flake marked by red circle) pristine, immediately exposed, post annealed, 6 day air exposed, and 14 day air exposed flake. Two MoS_2 Raman modes at 385 and 404 cm^{-1} depict broadening and shift of the 404 cm^{-1} peak.

high Raman enhancement is expected on ML MoS_2.[32,33] If there is any pyridine that may have adsorbed on the flake at room temperature, it would be desorbed by annealing to 150 °C. We have kept the annealing temperature low as thinning of MoS_2 starts at ~300 °C.[24,25] When MoS_2 flakes are exposed to a constant flow of pyridine vapor, there are quick interactions, namely, adsorption and desorption, between pyridine and MoS_2 at the adsorption−desorption equilibrium.[34,35] Our results indicate that electrons from strong n-type dopants, such as pyridine, are doped into the ML MoS_2 during these interactions. The increased electron density quenches the PL by destabilizing the excitons through charge screening.[12,36] As incident photons excite the electrons into the conduction band, the heavily filled conduction band screens the charges. Most of the photoexcited electrons and holes are forced to recombine nonradiatively via the Auger process. Charge screening destabilizes both excitons and trions; therefore, the PL intensity is low. A similar low PL intensity has been observed for 1T MoS_2.[7,37] On the other hand, charge accumulation is necessary for trions but not for neutral excitons. Therefore, although the intensity is very low, there is A^- trion emission remaining.

The PL of MoS_2 had recovered in time with exposure to the atmosphere at room temperature (Figure 1e) but very slowly. After 6 days in air, the PL had recovered about 5% of its original integrated intensity. The ML again has higher emission than the bilayer. The bilayer emission recovered slightly, only 2% that of the original integrated intensity.

Previous research shows that orders of magnitude higher carrier concentrations are doped in MoS_2 films by surface-stabilized self-assembly of amine-based polymer films formed by liquid chemistry methods.[38] When the amine-based film is removed from the MoS_2 by annealing at 300 °C in vacuum, the initial electronic properties recover. Recently, Friedman et al. have shown compelling evidence of the semiconductor−metal 2H−1T TMD phase transition when ML MoS_2 and $MoSe_2$ films are exposed to strong electron-donor chemical vapor analytes, namely, butylamine or trimethylamine.[16] In contrast to the continuous chemical doping via self-assembly polymer, these strong electron donors spontaneously desorb from the MoS_2 under ambient conditions. The phase transition, which is accompanied by a quenching of the PL intensity, is persistent, although the donor molecules desorb. In the work of Friedman et al., the semiconducting properties of ML MoS_2 are fully recovered only upon annealing to 400 °C in vacuum and when the basal plane is returned to the 2H phase.[16] In our experiments, MoS_2 flakes were not annealed above 150 °C in air to avoid oxidation and were not exposed to sufficient heating to cause relaxation of the 1T metallic phase. Since the ML MoS_2 flakes are on a nonconducting SiO_2/Si substrate, there is no immediate charge depletion. Our results suggest that the PL quenching is most likely caused by similar 1T phase transitions upon pyridine vapor exposure and that the slow recovery of PL is caused by a very gradual charge depletion of the MoS_2.

The charge transfer is further confirmed from the statistical analysis of Raman shifts. Raman maps (Figure 2) were taken from the flake before and after pyridine vapor exposure and after attempts to recover the PL. Figure 2a depicts the flake as a Raman intensity map with the Raman shift range including both the characteristic MoS_2 peaks at 383 and 405 cm^{-1}. They correspond to the E_{2g} in-plane Mo−S vibration mode and the A_{1g} out-of-plane Mo−S mode, respectively.[39] The Raman map of the pristine flake is of fairly uniform intensity all along the ML indicating that the flake is free of large-scale defects, which is consistent with its optical image. The signal from the middle of the flake is twice that of the surroundings, confirming the presence of the bilayer.

After pyridine exposure, annealing, and then air exposure for 6 days, the Raman map (Figure 2b) shows that the intensities of the Raman modes are unchanged, indicating that the flake is intact despite quenched PL. No pyridine Raman characteristic peaks were detected on any area of the flake after exposure nor were there any unknown Raman signals (Figure 2c). Further,

DOI: 10.1021/acs.jpcc.9b03277
J. Phys. Chem. C 2019, 123, 15738−15743

upon exposure to pyridine, a statistical analysis of the Raman peak positions throughout the entire MoS_2 flake (Figure 2c and Figure S1) shows that there was a 4 cm^{-1} red shift of the MoS_2 A_{1g} Raman peak. Since the shift is difficult to discern from an individual spectrum and could potentially be attributed to defects on ML MoS_2, a statistical analysis of ~300 Raman spectra collected from the entirety of the flake was done to properly examine the red shift. Subsequently, the peak position is calibrated with respect to the 520 cm^{-1} Si substrate lattice vibrational Raman mode.[40] The statistical analysis also shows that the peak height of the A_{1g} mode decreased and became broader. The red shift and the broadening of the A_{1g} mode are consistent with previously reported n-type doping, amine-based polymer film induced charge transfer to MoS_2.[38] The red shift is due to an increase of electrons in the conduction band of MoS_2, and the broadening is due to increased electron−phonon coupling. After annealing and then air exposure for 14 days, the red shift is reduced, and the A_{1g} nearly returns to its initial state, indicating that a certain amount of doping of the surface has been reversed and a percentage of carriers have relaxed. This is presumably related to the interaction of ambient molecules (O_2 and H_2O) with MoS_2, which introduces a p-doping process when the sample is in air for an extended time.[12,41] The p-doping process in air is slow and is less efficient than the n-doping process via pyridine. This is consistent with our previous study, which shows that photo-assisted reactions between the edge of the MoS_2 flake and air molecules (O_2 and H_2O) are needed for an effective p-doping and in turn increase the PL intensity at the edge.[23]

The E_{2g}^1 mode remains seemingly unchanged by pyridine exposure and annealing, but a statistical analysis of the peak position over 300 spectra throughout the entirety of the MoS_2 flake reveals that there is up to a 2 cm^{-1} blue shift of the peak upon exposure to pyridine vapor (Figure S1). This shift is close to the resolution of our instrument and not directly discernable from the spectra. This shift also gradually relaxes to its original position after annealing and air exposure for 14 days. This small shift is consistent with weaker electron−phonon coupling of the E_{2g}^1 mode in comparison to the A_{1g} mode.[6]

Interestingly, upon exposure to liquid pyridine, MoS_2 experienced a similar but reduced quenching effect. Figure 3a,b shows a fairly uniform reduction in the PL of an ML MoS_2 flake. Upon immersion in and subsequent evaporation of liquid pyridine, the total PL intensity is reduced by only 50% (Figure 3c) instead of by 99% when the flakes were exposed to gaseous pyridine. The trion and neutral exciton emissions are reduced slightly differentially to 45 and 55% of their original intensity (Figure 3c), respectively. The PL intensity from the bilayer has much less reduction and is only reduced by 12%. The results clearly show that the extent of charge transfer between liquid-phase pyridine and MoS_2 and that between gaseous-phase pyridine and MoS_2 is very different. This is attributed to the difference between liquid−surface and gaseous−surface interactions. The pyridine−pyridine interaction and pyridine−surface interaction compete at the heterogeneous interface. Pyridine is liquid at room temperature due to aromatic $\pi-\pi$ interactions of pyridine rings forming pyridine dimers.[42−47] The dimers show an antiparallel displaced structure with a 3.51 Å intermolecular distance between pyridine rings. Experimental and computational studies have shown that pyridine adsorbs flat on the perfect basal plane of the MoS_2 surface and interacts via weak van der Waals interaction.[32,34,48] However, various intrinsic defects and, in particular, high densities of sulfur vacancies have been experimentally observed on the basal plane of CVD-grown 2H-MoS_2 MLs.[49,50] Pyridine prefers to adsorb on defects and binds strongest when N is positioned in S-vacancies. A charge transfer from the pyridine to the MoS_2 system could occur with pyridine chemisorption.[48,51] Because the interaction of pyridine−pyridine in liquid is stronger than that in gas, the interaction between liquid pyridine molecules and the MoS_2 surface is not as strong as that in the gas-phase pyridine case. Further, the MoS_2 sample was kept under ventilation as the pyridine evaporated such that there was little chance for the evaporating pyridine monomers to interact with the MoS_2. In turn, the charge transfer between liquid pyridine and MoS_2 is less efficient.

The chemical doping is further studied by choosing thiophene, a molecule whose molecular structure and reactivity are similar to pyridine. Pristine ML MoS_2 flakes exposed to thiophene vapor experienced much less reduction (~50%, Figure 4) in PL than those exposed to pyridine vapor (~99%).

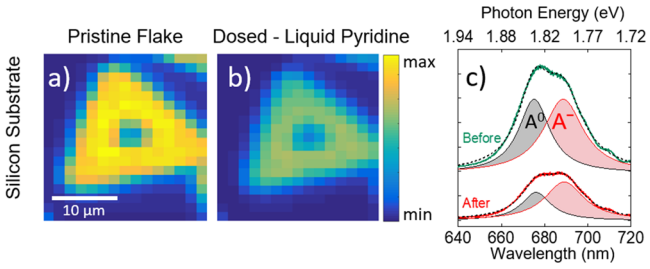

Figure 3. Photoluminescence (PL) quenching by liquid pyridine exposure. PL maps of MoS_2 flake on SiO_2/Si substrate (a) before and (b) after exposure to liquid pyridine. (c) Single representative PL spectrum from monolayer before and after exposure to liquid pyridine with deconvoluted spectra depicting the A^0 and A^- contributions to the overall PL intensity. The dashed black line is a fit of the PL spectra with deconvoluted A^0 and A^- shown as the gray and red infill, respectively, on both before and after PL spectra.

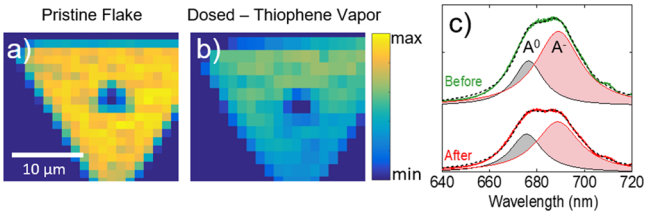

Figure 4. Photoluminescence (PL) quenching by thiophene vapor. PL maps of MoS_2 flake on silicon substrate (a) before and (b) after exposure to thiophene vapor. (c) Single PL spectrum taken from flake before and after thiophene exposure. The dashed black line is a fit of the PL spectra with deconvoluted A^0 and A^- contributions shown as the gray and red infill, respectively, on both before and after PL spectra.

Although both pyridine and thiophene molecules have a ring structure, the lone pair electrons on nitrogen in pyridine are not involved in the π conjugation in the ring. The lone pair on sulfur in thiophene is part of the π conjugation of the ring. The electronegativity of N is 3.04, and that of S is 2.58. Therefore, N can draw electrons from the ring, making pyridine a stronger electron donor than thiophene as shown in our results.[34] This

DOI: 10.1021/acs.jpcc.9b03277
J. Phys. Chem. C 2019, 123, 15738−15743

also supports that liquid pyridine is less efficient than gaseous pyridine in electron doping.

As many devices use conducting Au as a contact or substrate, we compared the difference between conductor and semiconductor substrates on the chemical doping induced PL quenching on MoS_2. The experiments were conducted on CVD-grown ML MoS_2 flakes that have been transferred to Au films. MoS_2 flakes on gold substrates in general show a much lower PL intensity, 2% of those on SiO_2/Si (Figure S2) due to band bending.[27,52] Upon exposure to pyridine vapor in a reaction cell, we observed PL quenching such that the extent of the PL quench (50% from initial PL) is less than that on the SiO_2/Si substrate. The resultant PL quenching of the already suppressed PL from MoS_2 indicates that the effect of the gas-phase dopant is consistent on different substrates and differentially prepared MoS_2. In addition, our results indicate that the excitation and emission of the excitons can be modulated by a combination of band bending and chemical doping on Au substrates (Figure S2).

Overall, our results suggest that monolayer MoS_2 flakes can be potentially used as a highly sensitive chemical sensor for detecting strong electron-donor chemicals. On the other hand, chemical doping has been used to modulate the optoelectronic properties of ML MoS_2 for potential applications such as ultrathin MoS_2 transistors, photodetectors, and switching devices. Our results show that a gaseous strong electron-donor dopant can completely quench PL. Therefore, it is necessary to protect ML MoS_2 from a gaseous strong electron-donor dopant during manufacturing and processing.

■ CONCLUSIONS

In summary, using in situ Raman microspectroscopy, we have demonstrated that the effect of a chemical dopant on the PL of CVD-grown monolayer MoS_2 strongly depends on the phase of the dopant. Specifically, gaseous pyridine, a strong electron donor, completely quenches the PL intensity (99%) of CVD-grown monolayer MoS_2. However, when exposed to liquid pyridine, only 50% of the PL is quenched, contributing to lower charge transfer efficiency to liquid over gaseous pyridine. This is attributed to the difference between liquid−surface and gaseous−surface interactions. The quenching is not reversible via annealing. When the gaseous dopant is changed to thiophene, a weaker electron-donor dopant, the extent of quenching is reduced. Our results suggest that monolayer MoS_2 flakes can be potentially used as a highly sensitive chemical sensor for detecting electron-donor chemicals.

■ ASSOCIATED CONTENT

Supporting Information

The Supporting Information is available free of charge on the ACS Publications website at DOI: 10.1021/acs.jpcc.9b03277.

Statistical analysis of Raman peak position of pyridine-vapor-dosed MoS_2, photoluminescence maps of MoS_2 on gold substrates dosed with pyridine vapor, and scanning tunneling microscope images of Au substrate surface (PDF)

■ AUTHOR INFORMATION

Corresponding Author

*E-mail: Zhenrong_Zhang@baylor.edu.

ORCID

Jonathan Hu: 0000-0001-6426-3051

Jun Lou: 0000-0002-0200-3948

Bert M. Weckhuysen: 0000-0001-5245-1426

Zhenrong Zhang: 0000-0003-3969-2326

Notes

The authors declare no competing financial interest.

■ ACKNOWLEDGMENTS

This work was supported by the National Science Foundation under Grant CHE-1609608. J.Y and J.L. acknowledge the support from Welch Foundation (grant C-1716) and the NSF I/UCRC Center for Atomically Thin Multifunctional Coatings (ATOMIC) under award no. IIP-1539999.

■ REFERENCES

(1) Kappera, R.; Voiry, D.; Yalcin, S. E.; Branch, B.; Gupta, G.; Mohite, A. D.; Chhowalla, M. Phase-Engineered Low-Resistance Contacts for Ultrathin MoS_2 Transistors. *Nat. Mater.* **2014**, *13*, 1128−1134.

(2) Sim, D. M.; Kim, M.; Yim, S.; Choi, M.-J.; Choi, J.; Yoo, S.; Jung, Y. S. Controlled Doping of Vacancy-Containing Few-Layer MoS_2 via Highly Stable Thiol-Based Molecular Chemisorption. *ACS Nano* **2015**, *9*, 12115−12123.

(3) Kiriya, D.; Tosun, M.; Zhao, P.; Kang, J. S.; Javey, A. Air-Stable Surface Charge Transfer Doping of MoS_2 by Benzyl Viologen. *J. Am. Chem. Soc.* **2014**, *136*, 7853−7856.

(4) Du, Y.; Liu, H.; Neal, A. T.; Si, M.; Ye, P. D. Molecular Doping of Multilayer MoS_2 Field-Effect Transistors: Reduction in Sheet and Contact Resistances. *IEEE Electron Device Lett.* **2013**, *34*, 1328−1330.

(5) Kang, D.-H.; Kim, M.-S.; Shim, J.; Jeon, J.; Park, H.-Y.; Jung, W.-S.; Yu, H.-Y.; Pang, C.-H.; Lee, S.; Park, J.-H. High-Performance Transition Metal Dichalcogenide Photodetectors Enhanced by Self-Assembled Monolayer Doping. *Adv. Funct. Mater.* **2015**, *25*, 4219−4227.

(6) Li, Y.; Xu, C.-Y.; Hu, P.; Zhen, L. Carrier Control of MoS_2 Nanoflakes by Functional Self-Assembled Monolayers. *ACS Nano* **2013**, *7*, 7795−7804.

(7) Voiry, D.; Goswami, A.; Kappera, R.; e Silva, C. D. C. C.; Kaplan, D.; Fujita, T.; Chen, M.; Asefa, T.; Chhowalla, M. Covalent Functionalization of Monolayered Transition Metal Dichalcogenides by Phase Engineering. *Nat. Chem.* **2015**, *7*, 45−49.

(8) Rastogi, P.; Kumar, S.; Bhowmick, S.; Agarwal, A.; Chauhan, Y. S. Doping Strategies for Monolayer MoS_2 via Surface Adsorption: A Systematic Study. *J. Phys. Chem. C* **2014**, *118*, 30309−30314.

(9) Wu, C.-C.; Jariwala, D.; Sangwan, V. K.; Marks, T. J.; Hersam, M. C.; Lauhon, L. J. Elucidating the Photoresponse of Ultrathin MoS_2 Field-Effect Transistors by Scanning Photocurrent Microscopy. *J. Phys. Chem. Lett.* **2013**, *4*, 2508−2513.

(10) Gan, L.-Y.; Zhang, Q.; Cheng, Y.; Schwingenschlögl, U. Photovoltaic Heterojunctions of Fullerenes with MoS_2 and WS_2 Monolayers. *J. Phys. Chem. Lett.* **2014**, *5*, 1445−1449.

(11) Le, Q. V.; Nguyen, T. P.; Jang, H. W.; Kim, S. Y. The Use of UV/Ozone-Treated MoS_2 Nanosheets for Extended Air Stability in Organic Photovoltaic Cells. *Phys. Chem. Chem. Phys.* **2014**, *16*, 13123−13128.

(12) Tongay, S.; Zhou, J.; Ataca, C.; Liu, J.; Kang, J. S.; Matthews, T. S.; You, L.; Li, J.; Grossman, J. C.; Wu, J. Broad-Range Modulation of Light Emission in Two-Dimensional Semiconductors by Molecular Physisorption Gating. *Nano Lett.* **2013**, *13*, 2831−2836.

(13) Mouri, S.; Miyauchi, Y.; Matsuda, K. Tunable Photoluminescence of Monolayer MoS_2 via Chemical Doping. *Nano Lett.* **2013**, *13*, 5944−5948.

(14) Coletti, C.; Riedl, C.; Lee, D. S.; Krauss, B.; Patthey, L.; von Klitzing, K.; Smet, J. H.; Starke, U. Charge Neutrality and Band-Gap Tuning of Epitaxial Graphene on SiC by Molecular Doping. *Phys. Rev. B* **2010**, *81*, 235401.

DOI: 10.1021/acs.jpcc.9b03277
J. Phys. Chem. C 2019, 123, 15738−15743

(15) Chen, W.; Chen, S.; Qi, D. C.; Gao, X. Y.; Wee, A. T. S. Surface Transfer p-Type Doping of Epitaxial Graphene. *J. Am. Chem. Soc.* **2007**, *129*, 10418−10422.
(16) Friedman, A. L.; Hanbicki, A. T.; Perkins, F. K.; Jernigan, G. G.; Culbertson, J. C.; Campbell, P. M. Evidence for Chemical Vapor Induced 2H to 1T Phase Transition in MoX_2 (X = Se, S) Transition Metal Dichalcogenide Films. *Sci. Rep.* **2017**, *7*, 3836.
(17) Eda, G.; Fujita, T.; Yamaguchi, H.; Voiry, D.; Chen, M.; Chhowalla, M. Coherent Atomic and Electronic Heterostructures of Single-Layer MoS_2. *ACS Nano* **2012**, *6*, 7311−7317.
(18) Eda, G.; Yamaguchi, H.; Voiry, D.; Fujita, T.; Chen, M.; Chhowalla, M. Photoluminescence from Chemically Exfoliated MoS_2. *Nano Lett.* **2011**, *11*, 5111−5116.
(19) Voiry, D.; Yamaguchi, H.; Li, J.; Silva, R.; Alves, D. C. B.; Fujita, T.; Chen, M.; Asefa, T.; Shenoy, V. B.; Eda, G.; et al. Enhanced catalytic activity in strained chemically exfoliated WS_2 nanosheets for hydrogen evolution. *Nat. Mater.* **2013**, *12*, 850−855.
(20) Gao, G.; Jiao, Y.; Ma, F.; Jiao, Y.; Waclawik, E.; Du, A. Charge Mediated Semiconducting-to-Metallic Phase Transition in Molybdenum Disulfide Monolayer and Hydrogen Evolution Reaction in New 1T′ Phase. *J. Phys. Chem. C* **2015**, *119*, 13124−13128.
(21) Cai, L.; Cheng, W.; Yao, T.; Huang, Y.; Tang, F.; Liu, Q.; Liu, W.; Sun, Z.; Hu, F.; Jiang, Y.; et al. High-Content Metallic 1T Phase in MoS_2-Based Electrocatalyst for Efficient Hydrogen Evolution. *J. Phys. Chem. C* **2017**, *121*, 15071−15077.
(22) Najmaei, S.; Liu, Z.; Zhou, W.; Zou, X.; Shi, G.; Lei, S.; Yakobson, B. I.; Idrobo, J.-C.; Ajayan, P. M.; Lou, J. Vapour Phase Growth and Grain Boundary Structure of Molybdenum Disulphide Atomic Layers. *Nat. Mater.* **2013**, *12*, 754−759.
(23) Birmingham, B.; Yuan, J.; Filez, M.; Fu, D.; Hu, J.; Lou, J.; Scully, M. O.; Weckhuysen, B. M.; Zhang, Z. Spatially-Resolved Photoluminescence of Monolayer MoS_2 under Controlled Environment for Ambient Optoelectronic Applications. *ACS Appl. Nano Mater.* **2018**, *1*, 6226−6235.
(24) Wu, J.; Li, H.; Yin, Z.; Li, H.; Liu, J.; Cao, X.; Zhang, Q.; Zhang, H. Layer Thinning and Etching of Mechanically Exfoliated MoS_2 Nanosheets by Thermal Annealing in Air. *Small* **2013**, *9*, 3314−3319.
(25) Yamamoto, M.; Einstein, T. L.; Fuhrer, M. S.; Cullen, W. G. Anisotropic Etching of Atomically Thin MoS_2. *J. Phys. Chem. C* **2013**, *117*, 25643−25649.
(26) Bao, W.; Borys, N. J.; Ko, C.; Suh, J.; Fan, W.; Thron, A.; Zhang, Y.; Buyanin, A.; Zhang, J.; Cabrini, S.; et al. Visualizing Nanoscale Excitonic Relaxation Properties of Disordered Edges and Grain Boundaries in Monolayer Molybdenum Disulfide. *Nat. Commun.* **2015**, *6*, 7993.
(27) Su, W.; Kumar, N.; Mignuzzi, S.; Crain, J.; Roy, D. Nanoscale Mapping of Excitonic Processes in Single-Layer MoS_2 using Tip-Enhanced Photoluminescence Microscopy. *Nanoscale* **2016**, *8*, 10564−10569.
(28) Mak, K. F.; Lee, C.; Hone, J.; Shan, J.; Heinz, T. F. Atomically Thin MoS_2: A New Direct-Gap Semiconductor. *Phys. Rev. Lett.* **2010**, *105*, 136805.
(29) Ruckenstein, A. E.; Schmitt-Rink, S. Many-Body Aspects of the Optical Spectra of Bulk and Low-Dimensional Doped Semiconductors. *Phys. Rev. B* **1987**, *35*, 7551−7557.
(30) Splendiani, A.; Sun, L.; Zhang, Y.; Li, T.; Kim, J.; Chim, C.-Y.; Galli, G.; Wang, F. Emerging Photoluminescence in Monolayer MoS_2. *Nano Lett.* **2010**, *10*, 1271−1275.
(31) Temel, B.; Tuxen, A. K.; Kibsgaard, J.; Topsøe, N.-Y.; Hinnemann, B.; Knudsen, K. G.; Topsøe, H.; Lauritsen, J. V.; Besenbacher, F. Atomic-Scale Insight Into the Origin of Pyridine Inhibition of MoS_2-Based Hydrotreating Catalysts. *J. Catal.* **2010**, *271*, 280−289.
(32) Muehlethaler, C.; Considine, C. R.; Menon, V.; Lin, W.-C.; Lee, Y.-H.; Lombardi, J. R. Ultrahigh Raman Enhancement on Monolayer MoS_2. *ACS Photonics* **2016**, *3*, 1164−1169.
(33) Ling, X.; Fang, W.; Lee, Y.-H.; Araujo, P. T.; Zhang, X.; Rodriguez-Nieva, J. F.; Lin, Y.; Zhang, J.; Kong, J.; Dresselhaus, M. S. Raman Enhancement Effect on Two-Dimensional Layered Materials: Graphene, h-BN and MoS_2. *Nano Lett.* **2014**, *14*, 3033−3040.
(34) Moses, P. G.; Mortensen, J. J.; Lundqvist, B. I.; Nørskov, J. K. Density Functional Study of the Adsorption and van der Waals Binding of Aromatic and Conjugated Compounds on the Basal Plane of MoS_2. *J. Chem. Phys.* **2009**, *130*, 104709.
(35) Masel, R. I. *Principles of Adsorption and Reaction on Solid Surfaces*; Wiley: New York, 1996.
(36) Newaz, A. K. M.; Prasai, D.; Ziegler, J. I.; Caudel, D.; Robinson, S.; Haglund, R. F., Jr.; Bolotin, K. I. Electrical Control of Optical Properties of Monolayer MoS_2. *Solid State Commun.* **2013**, *155*, 49−52.
(37) Zhang, J.; Wu, J.; Guo, H.; Chen, W.; Yuan, J.; Martinez, U.; Gupta, G.; Mohite, A.; Ajayan, P. M.; Lou, J. Unveiling Active Sites for the Hydrogen Evolution Reaction on Monolayer MoS_2. *Adv. Mater.* **2017**, *29*, 1701955.
(38) Lockhart de la Rosa, C. J.; Phillipson, R.; Teyssandier, J.; Adisoejoso, J.; Balaji, Y.; Huyghebaert, C.; Radu, I.; Heyns, M.; De Feyter, S.; De Gendt, S. Molecular Doping of MoS_2 Transistors by Self-Assembled Oleylamine Networks. *Appl. Phys. Lett.* **2016**, *109*, 253112.
(39) Ataca, C.; Topsakal, M.; Aktürk, E.; Ciraci, S. A Comparative Study of Lattice Dynamics of Three- and Two-Dimensional MoS_2. *J. Phys. Chem. C* **2011**, *115*, 16354−16361.
(40) Parker, J. H.; Feldman, D. W.; Ashkin, M. Raman Scattering by Silicon and Germanium. *Phys. Rev.* **1967**, *155*, 712−714.
(41) Nan, H.; Wang, Z.; Wang, W.; Liang, Z.; Lu, Y.; Chen, Q.; He, D.; Tan, P.; Miao, F.; Wang, X.; et al. Strong Photoluminescence Enhancement of MoS_2 through Defect Engineering and Oxygen Bonding. *ACS Nano* **2014**, *8*, 5738−5745.
(42) Gamba, Z.; Klein, M. L. A Molecular Dynamics Study of the Crystalline and Liquid Phases of Pyridine. *Chem. Phys.* **1989**, *130*, 15−22.
(43) Sagarik, K.; Spohr, E. Statistical Mechanical Simulations on Properties of Liquid Pyridine. *Chem. Phys.* **1995**, *199*, 73−82.
(44) Bakó, I.; Radnai, T.; Pálinkás, G. Investigation of the Structure of Liquid Pyridine: a Molecular Dynamics Simulation, an RISM, and an X-ray Diffraction Study. *Z. Naturforsch.* **1996**, *51*, 859−866.
(45) Trumpakaj, Z.; Linde, B. Molecular Dynamics Simulation of Pyridine. *J. Mol. Struct.* **2015**, *1085*, 268−275.
(46) Jorgensen, W. L.; McDonald, N. A. Development of an All-Atom Force Field for Heterocycles. Properties of Liquid Pyridine and Diazenes. *J. Mol. Struct.* **1998**, *424*, 145−155.
(47) Nagasaka, M.; Yuzawa, H.; Kosugi, N. Intermolecular Interactions of Pyridine in Liquid Phase and Aqueous Solution Studied by Soft X-ray Absorption Spectroscopy. *Z. Phys. Chem.* **2018**, *232*, 705−722.
(48) Logadóttir, Á.; Moses, P. G.; Hinnemann, B.; Topsøe, N.-Y.; Knudsen, K. G.; Topsøe, H.; Nørskov, J. K. A Density Functional Study of Inhibition of the HDS Hydrogenation Pathway by Pyridine, Benzene, and H_2S on MoS_2-Based Catalysts. *Catal. Today* **2006**, *111*, 44−51.
(49) Hong, J.; Hu, Z.; Probert, M.; Li, K.; Lv, D.; Yang, X.; Gu, L.; Mao, N.; Feng, Q.; Xie, L.; et al. Exploring Atomic Defects in Molybdenum Disulphide Monolayers. *Nat. Commun.* **2015**, *6*, 6293.
(50) Zhou, W.; Zou, X.; Najmaei, S.; Liu, Z.; Shi, Y.; Kong, J.; Lou, J.; Ajayan, P. M.; Yakobson, B. I.; Idrobo, J.-C. Intrinsic Structural Defects in Monolayer Molybdenum Disulfide. *Nano Lett.* **2013**, *13*, 2615−2622.
(51) Gainza, A. E.; Rodríguez-Arias, E. N.; Ruette, F. Pyridine Adsorption on a MoS_2 modelled Surface (Mo_3S_8). A CNDO Molecular Orbital Study. *J. Mol. Catal.* **1993**, *85*, 345−359.
(52) Bhanu, U.; Islam, M. R.; Tetard, L.; Khondaker, S. I. Photoluminescence Quenching in Gold - MoS_2 Hybrid Nanoflakes. *Sci. Rep.* **2014**, *4*, 5575.

DOI: 10.1021/acs.jpcc.9b03277
J. Phys. Chem. C 2019, 123, 15738−15743